Supporting Online Material for

Tuning the Activation Threshold of a Kinase Network by Nested Feedback Loops

Quincey A. Justman, Zach Serber, James E. Ferrell Jr., Hana El-Samad,* Kevan M. Shokat*

*To whom correspondence should be addressed. E-mail: helsamad@biochem.ucsf.edu (H.E.); shokat@cmp.ucsf.edu (K.M.S.)

Published 24 April 2009, *Science* **324**, 509 (2009)
DOI: 10.1126/science.1169498

This PDF file includes:

1. Materials and Methods

Oocyte culture. Stage VI oocytes were identified by size and morphology, then manually dissected away from *Xenopus* ovary tissue (Nasco). Isolated oocytes were cultured at 18˚C in Oocyte Ringer's solution 2 (OR2: 82.5mM NaCl, 2.5mM KCl, 1mM Na_2HPO_4•$7H_20$, 5mM Hepes, 1mM $CaCl_2$•$2H_20$, 1mM $MgCl_2$•$6H_20$, pH 7.8) supplemented with antibiotics. All experiments were initiated 24 to 48 hours after dissection. All experiments were carried out at 18˚C.

Sample preparation and single-cell western blotting. Individual oocytes were lysed by physical disruption in 20µL ice-cold lysis buffer (65mM Tris pH 7.5, 50mM NaF, 40mM β-glycerophosphate, 10mM EDTA, 10mM Na-pyrophosphate pH 7.2, 1mM $NaVO_4$) supplemented with fresh DTT (5mM), protease inhibitors (Complete tablets, Roche) and phosphatase inhibitors (Phosphatase Inhibitor Cocktails 1 and 2, Sigma). Lysed cells were centrifuged at 20,800 x *g* for 20 min. at 4˚C to pellet cell debris and float each oocyte's yolk layer. Clarified lysate (15µL) was collected between the cell pellet and the yolk, then boiled in Laemmli's Sample Buffer and used for western blotting. Prepared this way, each oocyte contained enough lysate for 2.5 lanes on a Criterion SDS-PAGE gel (Biorad).

Western blots were conducted using the Criterion-XT system (Biorad). Gels were run in MES buffer. The following primary antibodies were used for western blotting: phospho-GSK-3β Ser9 Santa Cruz Biotechnology sc-11757-R (1:500 to 1:1000 dilution in TBST+5% BSA); phospho-MAPK/ERK Tyr204 Santa Cruz Biotechnology sc-7976 (anti-goat, 1:2500 dilution in

TBST+5% BSA) and sc-7976-R (rabbit, 1:10,000 to 1:20,000 dilution in TBST+5% BSA); phospho-Cdk1 Tyr 15 Cell Signaling Technology #9111 (1:1000 dilution in TBST+5% BSA); Mos^{Xe} Santa Cruz Biotechnology sc-86 (1:1000 in TBST+5% powdered skim milk); total GSK-3β Cell Signaling Technology #9332 (1:1000 dilution in TBST+5% BSA). All primary antibody incubations were done overnight at 4˚C. All secondary antibodies were conjugated to HRP. Blots were developed using SuperSignal West Dura and SuperSignal West Femto reagents (Thermo). Blots were quantitated by CCD camera using an Alpha Innotech Imaging System (ChemiImager 5500 software package) or standard densitometry (ImageJ). Care was taken to keep signal within the linear range of detection.

Dose-response experiments. Progesterone dose-responses comparing treatments were conducted in parallel using oocytes harvested from the same frog. Progesterone (Sigma P6149) was dissolved in dry EtOH (Goldshield) and serially diluted into dry EtOH to achieve working stocks that were 100-fold more concentrated than each final concentration. This method kept EtOH concentrations constant across all progesterone treatments; these working stocks were made fresh for each experiment. Working stocks were diluted 1:100 into OR2 to achieve the final progesterone concentration of each data point. Oocytes were added, then incubated overnight at 18˚C (typically, maturation is completed within 10 hr.). M-phase entry was scored visually (GVBD) at all progesterone concentrations and confirmed by single oocyte western blot at intermediate concentrations.

Small molecule treatments. For all small molecule experiments, the solvent vehicle was applied to control and experimental conditions in equal concentration. 7AIPM (EMD Biosciences

361553) was dissolved in DMSO as a 10mM stock and applied at a final concentration of 50μM. PD98059 (EMD Biosciences 513000) was dissolved in DMSO as a 30mM stock and applied at a final concentration of 150μM. Fresh Leu (Sigma L8912) was dissolved in OR2 as a 50mM stock and applied at a final concentration of 5mM. In experiments using small molecules, oocytes were pretreated with the small molecule or its vehicle overnight, prior to progesterone stimulus.

Miscellaneous. For the timecourse, a pool of oocytes was stimulated with 1.5μM progesterone. At timepoints indicated, 24 oocytes were removed, lysed as 4 pools of 6 oocytes (a modification of the lysis procedure described above), and western blotted. Data are reported as the average signal of the 4 pools at each timepoint, +/-S.D. For hysteresis experiments, mature oocytes were washed in successive baths of OR2 for more than 18hr., such that the effective dilution of any remaining membrane-bound progesterone would be greater than 10,000-fold. For microinjection experiments, oocytes were microinjected with Mos (2.75ng, J. Yue, JEF lab), Cyclin BΔ90 (110nM, J. Yue, JEF lab), and GST-GSK-3β (Cell Signaling Technology, #7436). Microinjection volumes did not exceed 50nL. As a negative control, oocytes were injected with each protein's buffer or water. Mos- and cyclin-injected oocytes were lysed when they displayed GVBD; GSK-3β-injected oocytes were allowed to recover from microinjection for approx. 30 min. then stimulated with 1.5μM progesterone overnight at 18˚C.

2. Mathematical Modeling

Experimental rationale. The following four models (Models 0 through 3) recapitulate the GSK-3β-dependent desensitization observed in Figure 1C and D. They also conform to three additional biological observations: 7AIPM treatment does not compromise irreversibility (Fig. S3); total cellular GSK-3β concentrations remain constant during maturation (Fig. S4); and 7AIPM treatment does not alter steady-state levels of Mos, phospho-MAPK, and phospho-Cdk1 (Fig. S5). Box 1 describes the experimental basis of each term in Model 1 (our feedback regulation model). Models 0 through 3 are based on Model 1. They refine the model proposed by Ferrell and co-workers (*1*) by including two major changes:

1. We explicitly model the stimulus dependent increase in Mos translation (*2*).
2. We explicitly model the dynamics of GSK-3β inactivation and GSK-3β-dependent inhibition of Mos translation.

The resulting models describe the dynamics of Mos (M), phosphorylated, stabilized Mos (M*), and dephosphorylated, activated GSK-3β (G*).

Feed-forward, double-negative regulation. This mathematical model generated the behavior shown in Fig. 2A (top right panel). Model 0 (feed-forward) is a set of three differential equations given by:

Model 0 (feed-forward)

$$\frac{dM}{dt} = k_{off}^{M^*} M^* - \gamma_M M - k_{on}^{M} M + f_{pos} \frac{{M^*}^{n_H}}{{M^*}^{n_H} + EC_{50}^{n_H}} + \frac{stim^n}{stim^n + {K_s}^n} \frac{k_{stim}}{1 + ({}^{G^*}/_{K_{G^*}})^{n_1}}$$

$$\frac{dM^*}{dt} = k_{on}^{M} M - k_{off}^{M^*} M^* - \gamma_{M^*} M^*$$

$$\frac{dG^*}{dt} = k_{on}^{G} \frac{(G_t - G^*)}{K_{M^*}^{n_2} + stim^{n_2}} - k_{off}^{G^*} G^*$$

In this model, we have assumed that total GSK-3β is constant and equal to G_t and can be in the phosphorylated, inactivated form (G) or dephosphorylated, active form (G*), with the transition to G* inhibited by stimulus.

Analysis of the native system and the system upon addition of the GSK-3β inhibitor, 7AIPM (G*=0), indicates that GSK-3β inhibition raises the system's response threshold.

We present a list of parameters used in these simulations, their values, and their descriptions in Table 1.

Feedback, double-negative regulation. This mathematical model generated the behavior shown in Fig. 2A (bottom right panel). It is shown graphically in Fig. S6. For a description of how Model 1 was constrained by experimental observations, see Box 1. Model 1 is a set of three differential equations given by:

Model 1 (feedback)

$$\frac{dM}{dt} = k_{off}^{M^*} M^* - \gamma_M M - k_{on}^{M} M + f_{pos} \frac{{M^*}^{n_H}}{{M^*}^{n_H} + EC_{50}^{n_H}} + \frac{stim^n}{stim^n + {K_s}^n} \frac{k_{stim}}{1 + ({}^{G^*}/_{K_{G^*}})^{n_1}} \quad (1)$$

$$\frac{dM^*}{dt} = k_{on}^{M} M - k_{off}^{M^*} M^* - \gamma_{M^*} M^* \quad (2)$$

$$\frac{dG^*}{dt} = k_{on}^{G} \frac{(G_t - G^*)}{K_{M^*}^{n_2} + {M^*}^{n_2}} - k_{off}^{G^*} G^* \quad (3)$$

In this model, we have assumed that total GSK-3β is constant and equal to G_t and can be in the phosphorylated, inactivated form (G) or dephosphorylated, active form (G*), with the transition to G* inhibited by M*.

Analysis of the native system and the system upon addition of the GSK-3β inhibitor, 7AIPM (G*=0), indicates that GSK-3β inhibition does not change the classes of dynamical behavior that the system can exhibit, but rather changes its response threshold (Fig. S7). We present a list of parameters used in these simulations, their values, and their descriptions in Table 2.

A raised threshold is a structural feature of GSK-3β-mediated double-negative feedback and independent of parameter choice

To prove that GSK-3β activity decreases responsiveness for all sets of model parameters, we examined the dependence of the steady-state value of M* on G* through equation (1) in Model 1 above. At steady state, the value of M* obeys:

$$k_{off}^{M^*}M^* - \gamma_M M - k_{on}^{M}M + f_{pos}\frac{{M^*}^{n_H}}{{M^*}^{n_H}+EC_{50}^{n_H}} + \frac{stim^n}{stim^n+{K_s}^n}\frac{k_{stim}}{1+({}^{G^*}/_{K_{G^*}})^{n_1}} = 0 \text{ (a)}$$

Also, M is given by

$$k_{on}^{M}M - k_{off}^{M^*}M^* - \gamma_{M^*}M^* = 0 \rightarrow M = \frac{k_{off}^{M^*}+\gamma_{M^*}}{k_{on}^{M}} \text{ (b)}$$

Replacing M in (a) with (b) and rearranging generates the following:

$$-(k_{off}^{M^*} + \frac{k_{on}^{M}+\gamma_M}{k_{on}^{M}}(k_{off}^{M^*}+\gamma_{M^*}))M^{*(n_H+1)} + (f_{pos}+F){M^*}^{n_H} - \left(\frac{k_{on}^{M}+\gamma_M}{k_{on}^{M}}(k_{off}^{M^*}+\gamma_{M^*})EC_{50}^{n_H} - k_{off}^{M^*}EC_{50}^{n_H}\right)M^*$$
$$+ F.EC_{50}^{n_H} = 0$$

Where $F = \frac{stim^n}{stim^n+{K_s}^n}\frac{k_{stim}}{1+({}^{G^*}/_{K_{G^*}})^{n_1}}$

To simplify notation, we define:

$A = k_{off}^{M^*} + \frac{k_{on}^{M}+\gamma_M}{k_{on}^{M}}(k_{off}^{M^*}+\gamma_{M^*})$

$B = \frac{k_{on}^{M}+\gamma_M}{k_{on}^{M}}(k_{off}^{M^*}+\gamma_{M^*})EC_{50}^{n_H} - k_{off}^{M^*}EC_{50}^{n_H}$

Given these definitions, the equation above becomes:

$$f(M^*,F) = -A.{M^*}^{(n_H+1)} + (f_{pos}+F){M^*}^{n_H} - B.M^* + F.EC_{50}^{n_H} = 0 \text{ (c)}$$

M* at steady-state is a root (or roots) of this polynomial, and we examined how this root(s) depends on F. Specifically, we proved (below) that when G*=0 (+7AIPM) the root(s) of the polynomial are larger than those when G*>0 (WT). This indicates that when G*=0, M* reaches a threshold at lower input concentrations than when G*>0 (see Fig. S8A for intuition). Since F is a decreasing function of G*, we proved that the root(s) of the

polynomial is an increasing function of F. Since S is one root of the polynomial (that M*=S is a steady-state of the system), this entailed proving that $\frac{\partial S}{\partial F} > 0$.

Notice that $f(M^*,F)$ has three sign changes, therefore it has 0, 1, or 3 positive and real roots according to Descartes rule of signs (concentration of M* should be positive and real). We proved that $\frac{\partial S}{\partial F} > 0$ in the case when the polynomial has 1 positive real root. The proof is essentially the same for the case when the polynomial has 3 roots, where the conclusions hold for the first and third roots which are the stable steady-states of the system.

Proof: Let S be a root of $f(M^*,F)$. Then $f(M^*,F)$ can be factored as $f(M^*,F) = -(M^* - S)P(M^*,F)$, where $P(M^*,F)$ is a polynomial of real negative or complex roots such that $P(S,F) > 0$. Differentiating this expression by using the chain rule generates:

$$\frac{\partial f(M^*,F)}{\partial F} = -[(M^* - S)\frac{\partial P(M^*,F)}{\partial F} + P(M^*,F)\left(-\frac{\partial S}{\partial F}\right)]$$

From (c),

$$\frac{\partial f(M^*,F)}{\partial F} = M^{*n_H} + EC_{50}^{n_H}$$

Therefore,

$$\frac{\partial f(M^*,F)}{\partial F} = -\left[(M^* - S)\frac{\partial P(M^*,F)}{\partial F} + P(M^*,F)\left(-\frac{\partial S}{\partial F}\right)\right] = M^{*n_H} + EC_{50}^{n_H}$$

Now, $\frac{\partial f(M^*,F)}{\partial F}|_{M^*=S} = -P(S,F)\left(-\frac{\partial S}{\partial F}\right) = P(S,F)\frac{\partial S}{\partial F} = S^{n_H} + EC_{50}^{n_H}$

Since $P(S,F)>0$, $S^{n_H} > 0$, and $EC_{50}^{n_H} > 0$, it follows that $\frac{\partial S}{\partial F} > 0$.

In short, this proof demonstrates that M* is largest (lower threshold) when F is largest. F is larger when G* is small, with the limiting case being G*=0, where this model exhibits the lowest input threshold.

Note 1: The proof justifies the observed relationship between the degree to which the threshold is raised and the parameters shown in Figure S8. For example, decreasing K_{M^*} or increasing k_{on}^{G} amounts to increasing G* and decreasing F, and hence decreasing the value of M* and increasing the threshold (Fig. S8B). At the same time, decreasing K_{G^*} effectively

amounts to increasing the susceptibility of the system to G*, also increasing the threshold (Fig. S8C).

Raising a threshold through double-negative feedback is independent of model details: alternative mathematical models

In Model 1, we have assumed that the transition of G to G* is inhibited by M*. An alternative inhibition of G* could be implemented through the activation of the reverse transition (G*→G) by M*. In this case, the model is given by:

Model 2 (feedback, option 2)

$$\frac{dM}{dt} = k_{off}^{M^*} M^* - \gamma_M M - k_{on}^{M} M + f_{pos} \frac{M^{*n_H}}{M^{*n_H} + EC_{50}^{n_H}} + \frac{stim^n}{stim^n + {K_s}^n} \frac{k_{stim}}{1 + ({}^{G^*}/_{K_{G^*}})^{n_1}}$$

$$\frac{dM^*}{dt} = k_{on}^{M} M - k_{off}^{M^*} M^* - \gamma_{M^*} M^*$$

$$\frac{dG^*}{dt} = k_{on}^{G}(G_t - G^*) - k_{off}^{G^*} G^* \frac{M^{*n_2}}{K_{M^*}^{n_2} + M^{*n_2}}$$

The model described by these equations also shows the same increase in progesterone responsiveness upon inactivation of G* (Fig. S9A, parameters in Table 2), indicating that this behavior is insensitive to the details of the modeling. Rather, this effect is the result of implementing GSK-3β -dependent inactivation of M*.

Note 2: The outcome of model 2 is not unexpected given the proof detailed in the previous section. Another variant of the model can assume that the inhibition of M* implemented by G* has an additive (rather than multiplicative) effect. That is

$$\frac{dM}{dt} = k_{off}^{M^*} M^* - \gamma_M M - k_{on}^{M} M + f_{pos} \frac{M^{*n_H}}{M^{*n_H} + EC_{50}^{n_H}} + \frac{stim^n}{stim^n + {K_s}^n} + \frac{k_{stim}}{1 + ({}^{G^*}/_{K_{G^*}})^{n_1}}$$

In this case, $F = \frac{stim^n}{stim^n + {K_s}^n} + \frac{k_{stim}}{1 + ({}^{G^*}/_{K_{G^*}})^{n_1}}$, and the proof carries in an identical fashion.

Model 3 (feedback, option 3)

It is possible that the inhibition of M* by G* is implemented through a G*-mediated increase in the rate of conversion of M* to M, rather than an inhibition of M production. In this case, the model equations are given by

$$\frac{dM}{dt} = -\gamma_M M - k_{on}^{M} M + f_{pos}\frac{M^{*n_H}}{M^{*n_H} + EC_{50}^{n_H}} + k_{off}^{M^*} M^* \left(\frac{G^{*n_1}}{K_{G^*}{}^{n_1} + G^{*n_1}} + k_{off_{basal}}^{M^*}\right) + \frac{stim^n}{stim^n + K_s{}^n}$$

$$\frac{dM^*}{dt} = k_{on}^{M} M - k_{off}^{M^*} M^* \left(\frac{G^{*n_1}}{K_{G^*}{}^{n_1} + G^{*n_1}} + k_{off\_basal}^{M^*}\right) - \gamma_{M^*} M^*$$

$$\frac{dG^*}{dt} = k_{on}^{G}(G_t - G^*) - k_{off}^{G^*} G^* \frac{M^{*n_2}}{K_{M^*}^{n_2} + M^{*n_2}}$$

This model is also capable of producing the lowered threshold observed in the data upon inhibition of G* (see Figure S9B, parameters in Table 2) .

Hypothetical Positive Feedback Model

Subsequent analysis reveals that a raised threshold is an inherent property of specifically double-negative feedback. Adding a second, hypothetical double-positive feedback loop to the core bistable switch has the opposite effect: a lowered threshold (Fig. S10, parameters from Table 3). The hypothetical double positive feedback model that can be implemented by hypothetical kinase, P, is given by:

Model 4 (hypothetical double-positive regulation)

$$\frac{dM}{dt} = k_{off}^{M^*} M^* - \gamma_M M - k_{on}^{M} M + f_{pos}\frac{M^{*n_H}}{M^{*n_H} + EC_{50}^{n_H}} + \frac{stim^n}{stim^n + K_s{}^n}\frac{k_{stim1}\,({}^{P^*}/_{K_{P^*}})^{n_1}}{1 + ({}^{P^*}/_{K_{P^*}})^{n_1}} + k_{stim2}\frac{stim^n}{stim^n + K_s{}^n}$$

$$\frac{dM^*}{dt} = k_{on}^{M} M - k_{off}^{M^*} M^* - \gamma_{M^*} M^*$$

$$\frac{dP^*}{dt} = k_{on}^{P}(P_t - P^*)\frac{M^{*n_2}}{K_{M^*}^{n_2} + M^{*n_2}} - k_{off}^{P^*}P^*$$

Note 3: Taken as a composite, our mathematical analysis reveals that given only two observations about a hypothetical protein, ***X***: 1) that ***X***'s regulation is bistable, and; 2) that inhibition of ***X*** lowers the system's response threshold, it can be concluded that ***X*** is an antagonist of the response and engaged in a regulatory, double-negative feedback loop.

3. Supplementary Figures and Legends

Fig. S1

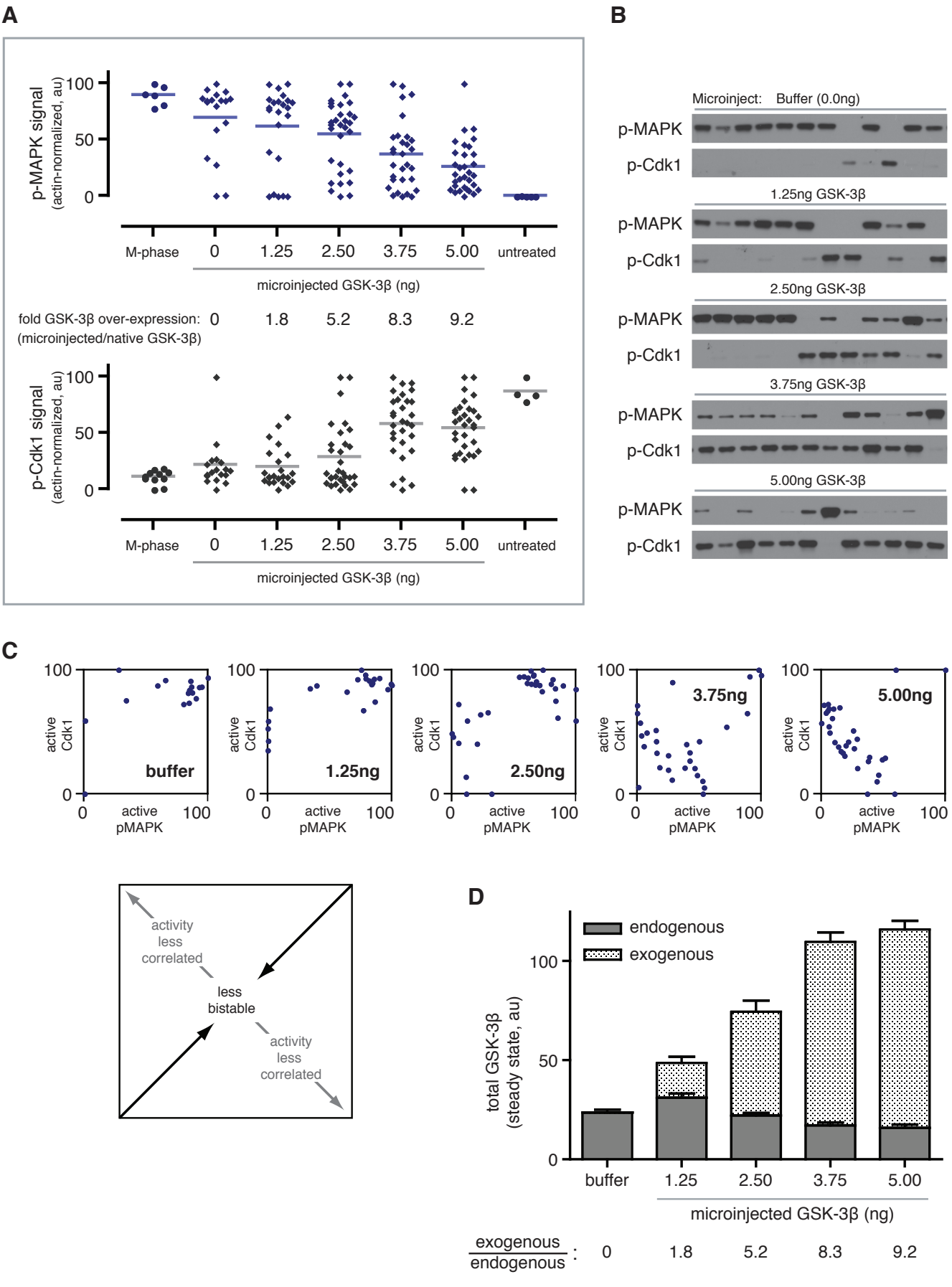

Fig. S2

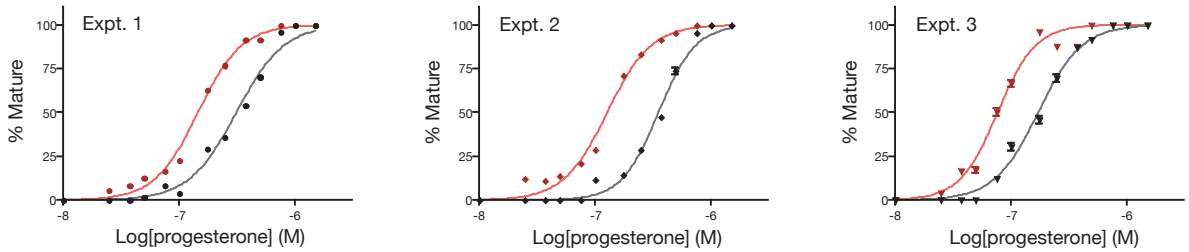

	Control			+GSK-3β Inhibition					
Expt.	Prog. EC_{50}	n_H	R^2	Prog. EC_{50}	n_H	R^2	n (Data point)	n (Total)	p-Value
1	316±4nM	2.12±0.06	0.98	147±2nM	2.31±0.04	0.99	12-48 oocytes	991 oocytes	p<0.0001
2	357±5nM	2.72±0.09	0.99	129±2nM	2.30±0.07	0.99	12-36 oocytes	684 oocytes	p<0.0001
3	173±3nM	2.29±0.07	0.99	77±15nM	2.67±0.12	0.98	12-24 oocytes	546 oocytes	p<0.0001

Fig. S3

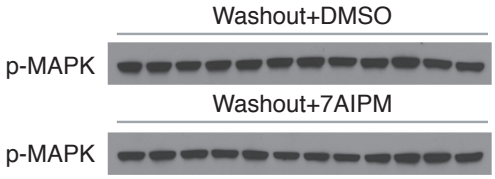

Fig. S4

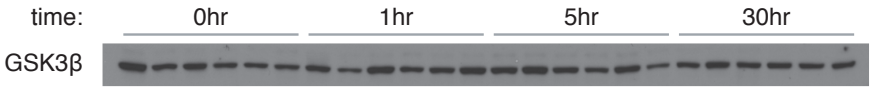

Fig. S5

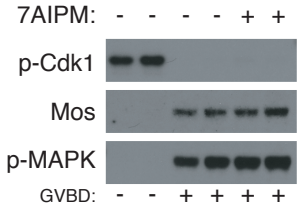

Fig. S6

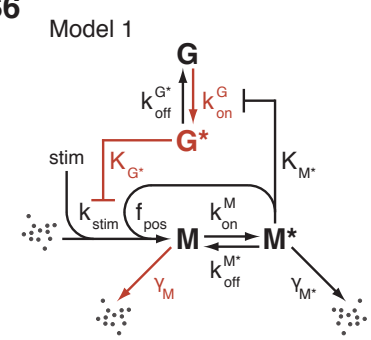

Fig. S7

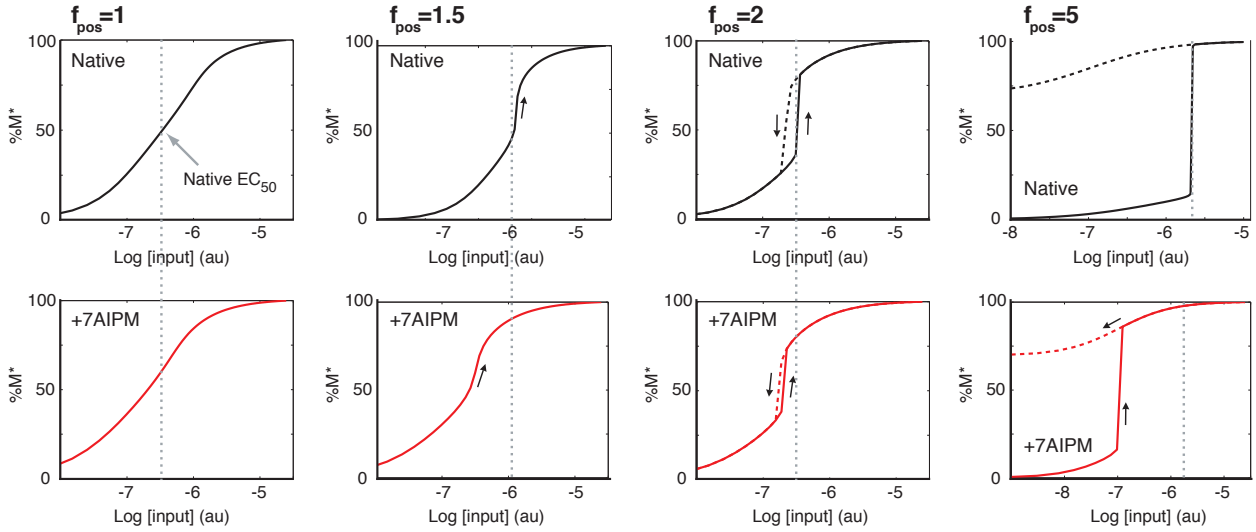

Fig. S8

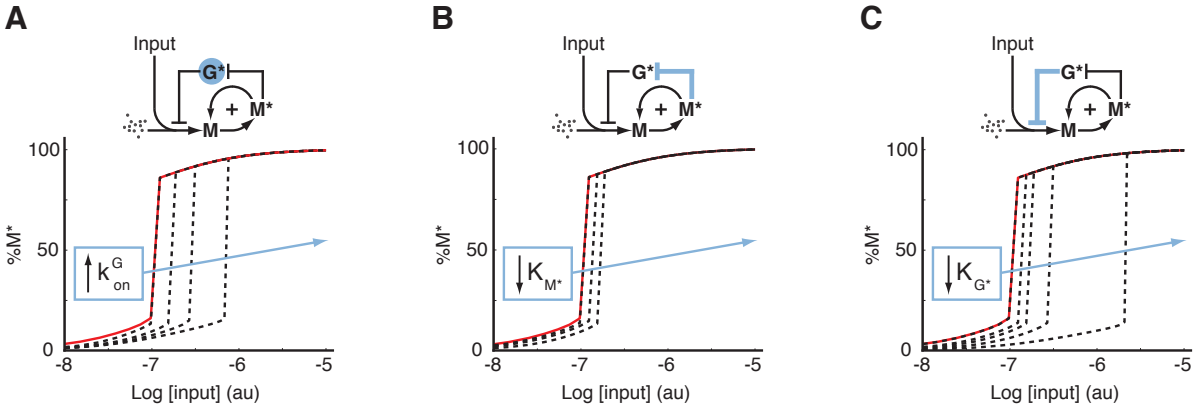

Flg. S9

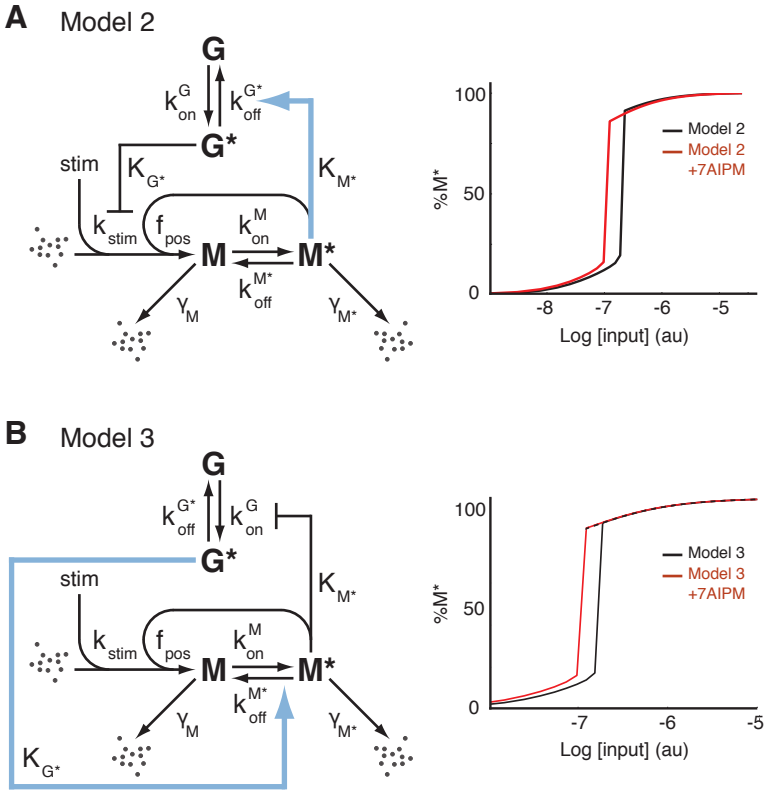

Fig. S10

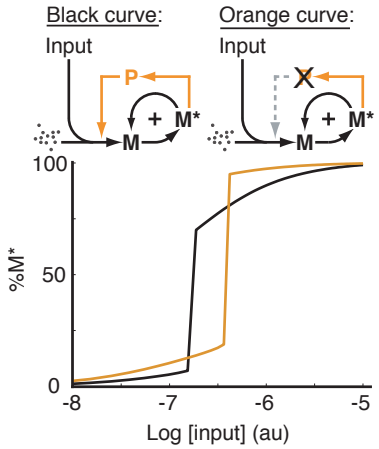

Figure S1. GSK-3β over-expression. Buffer or active GSK-3β protein was microinjected into oocytes prior to treatment with 1.5μM progesterone. Oocytes were lysed individually after overnight incubation with progesterone, then western blotted. Phospho-signals were quantitated, then normalized to actin levels to account for injury during microinjection **(A)**. "M-phase" designates oocytes that received progesterone stimulus only. Fold-overexpression of GSK-3β was calculated in Fig. S1D. **(B)** Western blots that generated the signals graphed in **A** (a representative sample of all oocytes scored). **(C)** Normalized phospho-Cdk1 and phospho-MAPK values obtained for Fig. S1A were plotted for each oocyte. Quantity of microinjected GSK-3β is indicated in ng. **(D)** Quantitation of GSK-3β over-expression in the microinjected oocytes. Endogenous GSK-3β and exogenous, GST-tagged GSK-3β were quantitated by CCD camera after western blotting.

Figure S2. Oocytes were induced to mature by progesterone treatment (concentration range: 1nM to 1μM); 7AIPM or DMSO was included in the progesterone solution during maturation. After 18hr, M-phase entry was scored visually (GVBD) at all progesterone concentrations and confirmed by single oocyte western blot at intermediate concentrations. Unscaled progesterone dose-responses from the three independent experiments compiled in Fig. 1B are plotted individually. Red and pink: 7AIPM-treated; black and grey: DMSO-treated. Error bars indicate S.E.M. The p-value for each experiment validates statistically significant differences between the EC_{50}'s of 7AIPM-treated and control (DMSO-treated) oocytes.

Figure S3. M-phase irreversibility during 7AIPM treatment. Oocytes were treated with 1μM progesterone for 18 hours +/- 100μM 7AIPM. After GVBD, oocytes were washed in multiple

baths for a total of 24 hours, then lysed individually. Where indicated, 7AIPM was added during maturation and the washout period. Lysates prepared from single oocytes were analyzed by western blot for phospho-p42MAPK.

Figure S4. Total GSK-3β levels during maturation. 3μM progesterone was added to oocytes; individual oocytes were lysed at the timepoints indicated. Total GSK-3β in each oocyte was scored.

Figure S5. Steady-state levels of M-phase markers during 7AIPM-treatment. DMSO-treated and 7AIPM-treated oocytes were stimulated with sub-maximal progesterone, lysed individually at steady-state, then western blotted as indicated.

Figure S6. Complete model of *Xenopus* oocyte maturation (Model 1). Terms in red dominate in the OFF state (interphase). For a description of all parameters and their initial conditions, see Table 2. For discussion of how experimental observations define the model structure, see Box 1.

Figure S7. The classes of dynamical behavior Model 1 can produce. Percent maturation as a function of progesterone concentration was modelled (Model 1) as the strength of Mos-dependent positive feedback was varied. As f_{pos} increases, the native (top) and +7AIPM (bottom) models transition from a graded response (left), to an all-or-none response with hysteresis (indicated with downward arrows and dashed lines) , then to an irreversible response (right, indicated with downward arrows and dashed lines). The behavior of the native model was originally described Supplemental Reference 1. The EC_{50} of the native system is indicated as a grey dotted line for each case.

Figure S8. The relationship between threshold and the strength of double-negative feedback. In all panels, the red curve depicts the behavior of the plus-7AIPM model shown in the main text (G*=0, Fig. 2A, bottom). Simplified switch topologies are indicated above. **(A)** As k_{on}^{G} approaches zero, the native network's behavior approaches the plus-7AIPM model. **(B)** As K_{M*} approaches infinity, the native network's behavior approaches the plus-7AIPM model. **(C)** As K_{G*} approaches zero, the native network's behavior approaches the plus-7AIPM model.

Figure S9. Threshold regulation by alternate modes of double-negative feedback. **(A)** Model 2. The black curve indicates the input dose-response curve of the native bistable system; the red curve models 7AIPM treatment (G*=0). A graphic description of Model 2 is at left; deviations from Model 1 are indicated in blue. **(B)** Model 3. The black curve indicates the input dose-response curve of the native bistable system; the red curve models 7AIPM treatment (G*=0). A graphic description of Model 3 is at left; deviations from Model 1 are indicated in blue.

Figure S10. Analysis of hypothetical double-positive feedback loop. Simplified switch topologies are indicated above. Modeling inhibition of the P-dependent branch of the hypothetical double-positive feedback produces the input dose-response curve in orange.

4. Box 1. Rationale behind each term of Model 1.

Model 1

$$\underset{\mathbf{A}}{\frac{dM}{dt}} = \underset{\mathbf{B}}{k_{off}^{M^*} M^*} - \underset{\mathbf{C}}{\gamma_M M} - \underset{\mathbf{D}}{k_{on}^{M} M} + \underset{\mathbf{E}}{f_{pos} \frac{{M^*}^{n_H}}{{M^*}^{n_H} + EC_{50}^{n_H}}} + \underset{\mathbf{F}}{\frac{stim^n}{stim^n + {K_s}^n} \frac{k_{stim}}{1 + ({}^{G^*}/_{K_{G^*}})^{n_1}}}$$

$$\underset{\mathbf{G}}{\frac{dM^*}{dt}} = \underset{\mathbf{H}}{k_{on}^{M} M} - \underset{\mathbf{I}}{k_{off}^{M^*} M^*} - \gamma_{M^*} M^*$$

$$\underset{\mathbf{J}}{\frac{dG^*}{dt}} = \underset{\mathbf{K}}{k_{on}^{G} \frac{(G_t - G^*)}{K_{M^*}^{n_2} + {M^*}^{n_2}} - k_{off}^{G^*} G^*}$$

Definitions: All interphase signaling is aggregated into the term *stim*; *M* is newly synthesized Mos; all Mos-dependent signaling is aggregated into the term *M**; *G** is active GSK-3β; k_{on} designates activation terms; k_{off} designates inactivation terms; γ designates destruction. To model 7AIPM treatment (Fig. 1C and 2A), *G** is set to zero.

Term	Definition	Rationale	Reference
A	Conversion of *M** to *M*		
B	Destruction of *M*	Assumption: the destruction rate of *M*>>>*M**. *This assumption allows for the accumulation of* M*, *analogous to Mos accumulation prior to meiotic entry in* Xenopus *oocytes.*	*Bioessays* **19**, 23, for example.
C	Conversion of *M* to *M**		
D	Production of *M* due to positive feedback	Assumption: *M* saturates. *As required by bistability, M-phase signals reach a stable maximum.* *This is the core of the Ferrell model. It generates bistable behavior.*	*Nature* **426**, 460, *Science* **280**, 895, and Fig. 2 and 3 of this work.
E	Stimulus-dependent accumulation of *M*	Assumption: *M* saturates. *Mos levels reach a maximum* in vivo. *This term explicitly models Mos translation during meiotic entry.*	Fig. 2B of this paper and other published work.
F	Inhibition of *M* accumulation due to *G** activity	*This term describes the branch of double-negative feedback downstream of GSK-3β.*	This relationship was characterized in this work, Fig. S1, 2 and 3. See also *Genes Dev* **18**, 48.
G	Conversion of *M* to *M**		
H	Conversion of *M** to *M*		
I	Destruction of *M**	Assumption: the destruction rate of *M*>>>*M**. *See also* **A**, *above.*	Fig. 2B shows Mos accumulation. Also see *Bioessays* **19**, 23.
J	*G** activation, scaled by 1/*M**	*This term describes the branch of double-negative feedback upstream of GSK-3β.*	This relationship was discovered in this work as described in Fig. 2 and 3.
K	Inactivation of *G**	G_t *levels are constant, as we observe* in vivo.	Fig. S4 of this work.

5. Tables of Parameter Values

Table 1: Parameters for Model 0.

Parameter	Value	Significance
$Stim$	varied	Progesterone stimulus
G_t	15	Total GSK-3β (G+G*)
G	0	Phosphorylated, inactive GSK-3β
G^*	15	Dephosphorylated, active GSK-3β
M	0	Dephosphorylated, inactive Mos
M^*	0	Phosphorylated, stabilized, active Mos
$k_{off}^{M^*}$	0.1	Rate of Mos dephosphorylation
k_{on}^{M}	0.2	Rate of Mos phosphorylation
γ_M	0.1	Degradation rate of dephosphorylated Mos
γ_{M^*}	0.01	Degradation rate of phosphorylated Mos
f_{pos}	5	Maximal strength of Mos-dependent positive feedback
n_H	5	Hill coefficient of Mos-dependent positive feedback, value reported in *Science* **280**, 895 and *Nature* **426**, 460.
EC_{50}	35	Progesterone concentration that elicits half-maximal active Mos, derived from *in vivo* measurements in this study (Fig. S2)
$k_{off}^{G^*}$	0.1	Rate of GSK-3β phosphorylation
k_{stim}	2	Maximal rate progesterone-stimulated Mos translation
n_1	3	Hill coefficient of Mos translation
K_{G^*}	12	GSK-3β concentration that elicits half-maximal inhibition of Mos translation, calculated to recapitulate the *in vivo* data of Fig. S2.

k_{on}^{G}	2	Maximal rate of GSK-3β activation, calculated to recapitulate the *in vivo* data of Fig. S2.
n_2	1	Hill coefficient of Mos's inhibition of GSK-3β activation
K_{M^*}	19	Mos concentration that elicits half-maximal inhibition of GSK-3β activation, calculated to recapitulate the *in vivo* data of Fig. S2.
n	2	Hill coefficient of stimulus
K_s	0.95	Stimulus concentration that elicits half maximal Mos translation

Table 2: Parameters for Models 1-3.

Parameter	Value	Significance
$Stim$	varied	Progesterone stimulus
G_t	15	Total GSK-3β (G+G*)
G	0	Phosphorylated, inactive GSK-3β
G^*	15	Dephosphorylated, active GSK-3β
M	0	Dephosphorylated, inactive Mos
M^*	0	Phosphorylated, stabilized, active Mos
$k_{off}^{M^*}$	0.1	Rate of Mos dephosphorylation
k_{on}^{M}	0.2	Rate of Mos phosphorylation
γ_M	0.1	Degradation rate of dephosphorylated Mos
γ_{M^*}	0.01	Degradation rate of phosphorylated Mos
f_{pos}	5	Maximal strength of Mos-dependent positive feedback
n_H	5	Hill coefficient of Mos-dependent positive feedback, value reported in *Science* **280**, 895 and *Nature* **426**, 460.

EC_{50}	35	Progesterone concentration that elicits half-maximal active Mos, derived from *in vivo* measurements in this study (Fig. S2)
$k_{off}^{G^*}$	0.1	Rate of GSK-3β phosphorylation
k_{stim}	2	Maximal rate progesterone-stimulated Mos translation
n_1	3	Hill coefficient of Mos translation
K_{G^*}	12	GSK-3β concentration that elicits half-maximal inhibition of Mos translation, calculated to recapitulate the *in vivo* data of Fig. S2.
k_{on}^{G}	2	Maximal rate of GSK-3β activation, calculated to recapitulate the *in vivo* data of Fig. S2.
n_2	1	Hill coefficient of Mos's inhibition of GSK-3β activation
K_{M^*}	1	Mos concentration that elicits half-maximal inhibition of GSK-3β activation, calculated to recapitulate the *in vivo* data of Fig. S2.
n	2	Hill coefficient of stimulus
K_s	0.95	Stimulus concentration that elicits half maximal Mos translation

Table 3: Parameters for Model 4.

Parameter	Value	Significance
Stim	varied	Progesterone stimulus
P_t	15	Total P (P+P*)
P	0	Inactive P
P^*	15	Active P
M	0	Dephosphorylated, inactive Mos
*M**	0	Phosphorylated, stabilized, active Mos

$k_{off}^{M^*}$	0.1	Rate of Mos dephosphorylation
k_{on}^{M}	0.2	Rate of Mos phosphorylation
γ_M	0.1	Degradation rate of dephosphorylated Mos
γ_{M^*}	0.01	Degradation rate of phosphorylated Mos
f_{pos}	5	Maximal strength of Mos-dependent positive feedback
n_H	5	Hill coefficient of Mos-dependent positive feedback, value reported in *Science* **280**, 895 and *Nature* **426**, 460.
EC_{50}	35	Progesterone concentration that elicits half-maximal active Mos, derived from *in vivo* measurements in this study (Fig. S2)
$k_{off}^{P^*}$	1	Rate of P^* inactivation
k_{stim1}	60	Maximal rate of progesterone-stimulated Mos translation
k_{stim2}	1.3	Amplification of stimulus
n_1	3	Hill coefficient of Mos activation
K_{P^*}	12	P concentration that elicits half-maximal induction of Mos translation
k_{on}^{P}	1	Rate of P activation
n_2	1	Hill coefficient of Mos's induction of P activation
K_{M^*}	100	Mos concentration that elicits half-maximal P activation
n	2	Hill coefficient of stimulus
K_s	0.95	Stimulus concentration that elicits half maximal Mos translation

6. Supplemental References

1. W. Xiong, J. E. Ferrell, Jr., *Nature* **426**, 460 (Nov 27, 2003).
2. N. Sagata, M. Oskarsson, T. Copeland, J. Brumbaugh, G. F. Vande Woude, *Nature* **335**, 519 (Oct 6, 1988).